Photoacoustics 28 (2022) 100423

Contents lists available at ScienceDirect

Photoacoustics

journal homepage: www.elsevier.com/locate/pacs

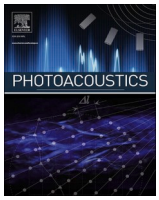

Cantilever-enhanced photoacoustic spectroscopy for gas sensing: A comparison of different displacement detection methods

Yonggang Yin, Danyang Ren, Chiye Li, Ruimin Chen, Junhui Shi *

Research Center for Humanoid Sensing, Zhejiang Laboratory, Hangzhou 311100, China

ARTICLE INFO

Keywords:
Photoacoustic spectroscopy
Cantilever-enhanced
Displacement detection
Trace gas detection
Acoustic sensor

ABSTRACT

Photoacoustic spectroscopy (PAS) combines the advantages of high sensitivity, high specificity and zero background, which is very suitable for trace gas detection. Cantilever-enhanced photoacoustic spectroscopy (CEPAS) utilizes highly sensitive mechanical cantilevers to further enhance the photoacoustic signal and shows a gas concentration detection limit of parts per trillion. This review is intended to summarize the recent advancements in CEPAS based on different displacement detection methods, such as Michelson interference, Fabry-Perot interference, light intensity detection, capacitive, piezoelectric and piezoresistive detection. Fundamental mechanisms and technical requirements of CEPAS are also provided in the literature. Finally, potential challenges and further opportunities are also discussed.

1. Introduction

High-sensitivity trace gas detection is important in many fields, such as measurement of trace air pollutants, monitoring of gases produced in industrial processes, detection of toxic, harmful and explosive gas leakage, and human biomarkers test in breath to diagnose diseases [1–3]. Measurement methods of gas concentration are mainly divided into non-optical methods and optical methods [4]. Non-optical methods include chromatography, mass spectrometry, chemical sensors, semiconductor sensors, etc. Chromatography and mass spectrometry have high sensitivity, but the acquisition and processing time is long, which is not suitable for real-time measurement. Chemical and semiconductor sensors are portable and cheap, but the stability, specificity and sensitivity are poor. Optical methods based on optical absorption detection, such as tunable diode laser absorption spectroscopy (TDLAS) [5], cavity ring-down spectroscopy (CRDS) [6] and photoacoustic spectroscopy (PAS) [7–13], have high sensitivity and sharp specificity. TDLAS and CRDS measure the attenuated laser energy by photodetectors after gas absorption. Generally, they are usually with large volume because the sensitivity is proportional to the optical path length. Compared with other optical methods, PAS converts light energy into acoustic energy and then detects the signal by acoustic sensors, which overcomes the wavelength response limitation of the photoelectric detector and is theoretically unaffected by the background light (except for some photothermal noise). Besides, the acoustic sensors are usually compact and inexpensive compared to photoelectric detectors.

In order to further improve the signal to noise ratio (SNR) and sensitivity of PAS, several enhanced techniques have been developed in recent years, such as quartz-enhanced photoacoustic spectroscopy (QEPAS) [14–19] and cantilever-enhanced photoacoustic spectroscopy (CEPAS). The acoustic sensors utilized in QEPAS and CEPAS are quartz tuning fork and cantilever, respectively. In essence, QEPAS and CEPAS both use mechanical resonators to improve the sensitivity of acoustic detection. When the frequency of modulated acoustic wave and the natural frequency of mechanical resonator are equal, the output signal amplitude of PAS reaches the maximum. In QEPAS, the quartz tuning fork converts the vibration displacement into electric output through piezoelectric effect. The quality factor of the quartz tuning fork in the atmosphere can reach 10000, which produces great gain ratio at resonant frequency and makes the sensor insensitive to ambient noise. However, QEPAS is easily affected by the vibration-translation (V-T) relaxation process of some certain kinds of gases, such as CO_2 [20]. The commonly used standard quartz tuning forks are optimized for timing purposes, operating at ~32.7 kHz, instead of spectroscopic applications. The energy transfer of some gases cannot follow the fast molecular vibration excitation due to its relatively long relaxation time, which results in a weak signal output [20–23]. In CEPAS, the resonant frequency of the cantilevers can be easily designed by adjust the length, width or height, in order to adapt to gases with different relaxation rates.

It is important to note that the cantilever in CEPAS does not always

* Corresponding author.
E-mail address: junhuishi@zhejianglab.com (J. Shi).

https://doi.org/10.1016/j.pacs.2022.100423
Received 23 September 2022; Received in revised form 26 October 2022; Accepted 28 October 2022
Available online 31 October 2022

operate in resonant mode. The resonant frequency of the cantilever is proportional to the square root of its spring stiffness. Low-stiffness cantilevers are more prone to deformation, which enables the cantilever with low resonant frequency to obtain high sensitivity even in non-resonant working mode. In non-resonant mode, multiple wavelengths can be multiplexed to different frequencies to achieve simultaneous measurement of multi-component gases. In addition, the resonant frequency is sensitive to environmental factors, while the sensitivity of the cantilever in non-resonant mode is less affected.

The cantilevers can be fabricated by micro-electrical-mechanical system (MEMS) technologies, which can dramatically reduce the size and cost and is potential for on-chip integration of the entire gas detection system. The displacement of the cantilever can be readout by many methods, such as optical, piezoelectric, piezoresistive and capacitive methods. Optical readout methods have extremely high sensitivity for displacement detection while other methods have more advantages in miniaturization and integration.

In this review, we summarized the recent advances in several representative CEPAS, as well as their advantages and disadvantages. First, the theoretical basis of the CEPAS technique is introduced. Next, the principles and applications of different readout techniques used in CEPAS are reviewed. Finally, comparation, challenges and development prospects of CEPAS are highlighted in the conclusion section.

2. Basic principle of CEPAS

PAS is a kind of laser absorption spectroscopy based on photoacoustic effect. The basic principle is shown in Fig. 1. When the gas molecules absorb laser energy, their energy levels go from the ground state to the excited state. Then the excited state gas molecules go through a thermal relaxation process and increase the local pressure. If the laser energy is modulated, periodic thermal expansion will generate acoustic wave. In the early stage, PAS was realized by amplitude modulation (AM) through a mechanical chopper [24]. With the development of distributed feedback (DFB) lasers, wavelength modulation (WM) has become the dominant modulation method [25]. In AM-based PAS, the frequency of acoustic wave to be measured is equal to the frequency of laser modulation. The periodic heating of the photoacoustic cell walls and the optical windows will generate coherent acoustic noise in the same frequency, which cannot be suppressed by lock-in amplifier. This can be avoided in WM-based PAS by second harmonic detection (2 f detection), in which the frequency of acoustic wave to be measured is twice the frequency of laser modulation. A combination of sawtooth and sine waves is used to regulate the current of the DFB laser. The low-frequency sawtooth wave is used to scan wavelengths over a certain range, while the high-frequency sine wave is used to modulate the acoustic wave.

The generated acoustic wave can be detected by acoustic sensors, like commercial microphones. In CEPAS, a sensitive cantilever is used as the acoustic sensor. Because of the large displacement response at its resonant frequency, the cantilever beam is particularly suitable for single-frequency acoustic wave measurement in PAS. In resonant working mode, the frequency of the sine wave is equal to half of the resonant frequency of the cantilever (2 f detection) in Fig. 1. In non-resonant working mode, the frequency of the sine wave will be much smaller to obtain a flat frequency response. The displacement signal of the cantilever is measured by a lock-in amplifier and the sine wave is used as a reference. The lock-in amplifier includes an integrator and a low-pass filter, which can extract the signal amplitude near a specific frequency. Finally, a high SNR photoacoustic signal is obtained and transmitted to a computer.

There are two important parameters to evaluate the performance of the PAS system: the minimum detection limit (MDL) and the normalized noise equivalent absorption (NNEA). The MDL represents the minimum gas concentration that the system can detect. The MDL can be calculated by two methods. One is based on the SNR: the background noise level is the minimum detection limit under the actual test conditions. The other is according to Allan standard deviation: the lowest point of Allan standard deviation curve indicates the optimal detection ability that the system has the potential to achieve under filtering conditions [26]. The common units of the MDL include parts per million (ppm), parts per billion (ppb) and parts per trillion (ppt). The NNEA quantifies the performance of the sensor independently from the laser power, the gas line absorption strength and the equivalent noise bandwidth of the lock-in amplifier, thus allowing the comparison of different PAS systems even if the test conditions are not identical. The NNEA can be calculated according to the formula:

$$\mathrm{NNEA} = \frac{\alpha P}{\mathrm{SNR}\sqrt{\Delta f}}$$

where α is the absorption coefficient of the gas absorption line in cm^{-1}, which can be calculated using the HITRAN database [27], P is the optical power in W, SNR is the signal-to-noise ratio and Δf is the detection bandwidth in Hz, which is usually determined by the lock-in amplifier.

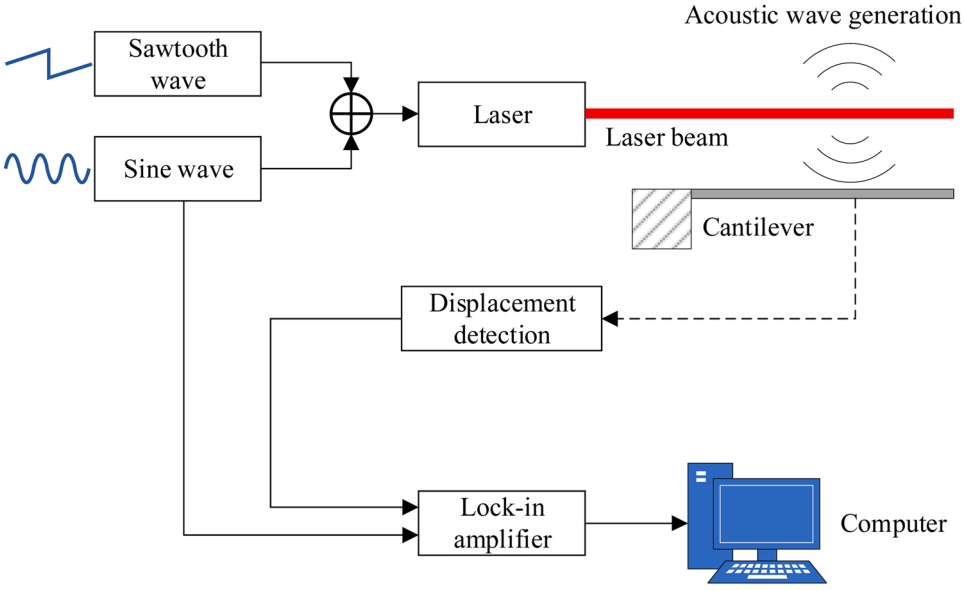

Fig. 1. Basic principle diagram of a WM-based CEPAS system.

The unit of the NNEA is $cm^{-1}WHz^{-1/2}$.

The key technologies of CEPAS are the design of high sensitivity cantilevers and high SNR displacement readout. Benefiting from the development of precision micro-machining technology and various displacement detection techniques, the measurement accuracy of CEPAS has been continuously improved.

3. CEPAS based on different displacement detection techniques

3.1. CEPAS based on optical detection

Optical detection methods have been proved to be highly accurate and sensitive for vibration measurement. They can work in high temperature, electromagnetic interference and other harsh environments. In

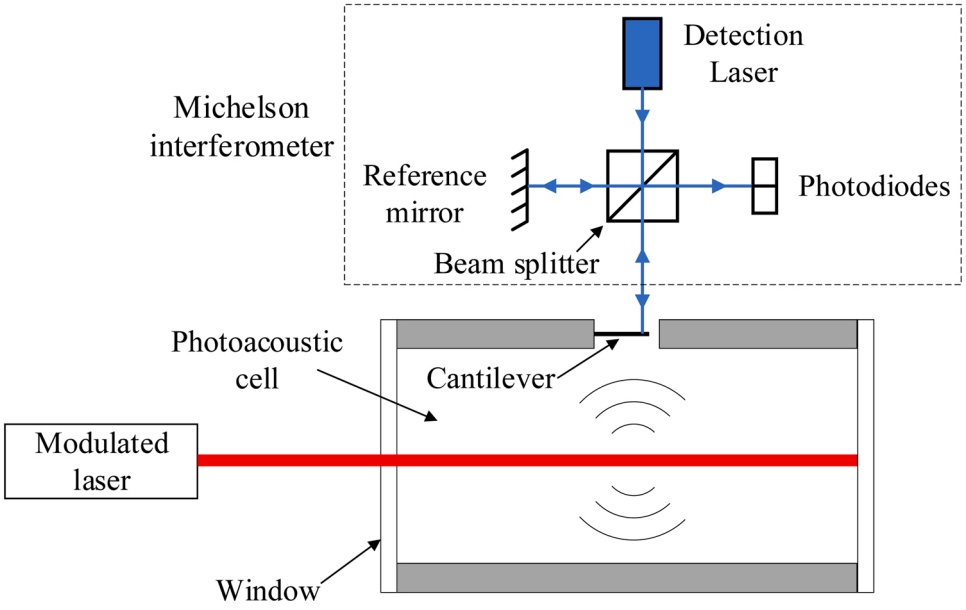

(a)

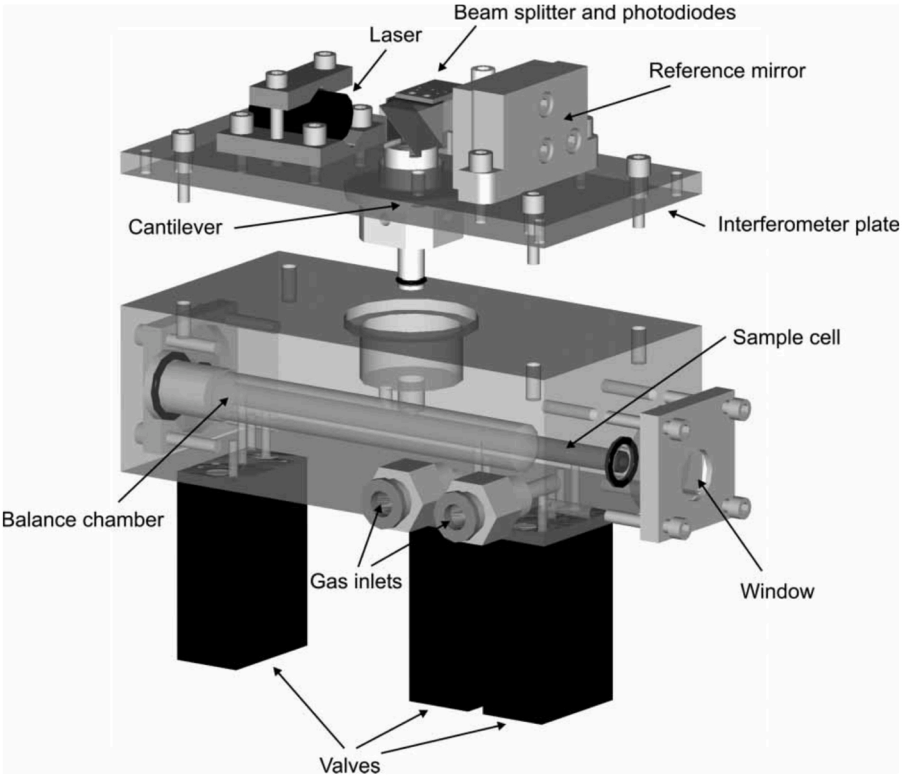

(b)

Fig. 2. Michelson interference based CEPAS. (a) A schematic view. (b) The realistic structure of the photoacoustic cell with the cantilever and the Michelson interferometer manufactured by Gasera Ltd [29].

CEPAS, optical detection is the most used displacement readout method and can be divided into three main types: Michelson interference (MI), Fabry-Perot interference (FPI) and light intensity detection.

(1) Michelson interference

In 2003, CEPAS was firstly reported by Wilcken and Kauppinen at University of Turku (Finland) and the motion of the cantilever was observed with a Michelson interferometer [28]. The sensitivity achieved with the optical cantilever microphone in the non-resonant mode was 100 times higher than with the commercial capacitive microphone. The basic construction of the photoacoustic system with a Michelson interferometric cantilever microphone is shown in Fig. 2(a). The principle of the Michelson interferometer is that a detection laser beam is divided into two beams by a splitter, then the two beams are respectively reflected back by the cantilever and a reference mirror, and finally detected by photodiodes. The optical path difference can be measured by the interference of the two beams very accurately. When the modulated laser is incident into the photoacoustic cell, the excited sound wave causes the cantilever beam to vibrate and then the displacement of the cantilever is detected by the Michelson interferometer.

Based on the work of Kauppinen et al., Gasera Ltd. (Turku, Finland) was founded in 2004. Gasera has developed a number of spectrum products based on CEPAS, the most classic model of which is PA201. As shown in Fig. 2(b), Gasera's custom gas measurement system is a gas cell with an integrated Michelson interferometer [29]. The sample cell (photoacoustic cell) is a long tube and the cantilever is positioned at the end of the narrow side tube attached at the middle of the sample tube. The interferometer is placed above the sample cell and the detection laser beam is directed downwards to the cantilever. This device can be combined with different types of laser sources, making it an extremely versatile tool for many researchers [29–49]. In 2007, Koskinen et al. used CEPAS to detect CO_2 at 1572 nm with a DFB laser [30] and the NNEA reached 1.7×10^{-10} $cm^{-1}WHz^{-1/2}$. McNaghten et al. reported a demonstration of simultaneous detection of multiple trace gases (CO, C_2H_2, CH_4 and CO + CO_2) by near-IR tunable diode laser (TDL) photoacoustic spectroscopy in 2012 [33]. Four fiber-coupled DFB TDLs with different wavelengths were used in the system and modulated at different frequencies. The NNEA ranging between 3.4×10^{-9} and 1.4×10^{-9} $cm^{-1}WHz^{-1/2}$ were obtained for multispecies detection. Peltola et al. combined CEPAS and a mid-infrared continuous-wave optical parametric oscillator (OPO) laser to detect HCN and CH_4 in 2013 [36]. MDL of 190 ppt (with an averaging time of 1 s) and 65 ppt (30 s) were achieved for HCN and CH_4, respectively, and the best NNEA (1σ) was 1.8×10^{-9} $cm^{-1}WHz^{-1/2}$. Hirschmann et al. used OPO to measure multi gases in 2013 [35]. The OPO was tunable from 3237 to 3296 nm in steps of 0.1 nm and the multivariate MDL (3σ, 0.951 s) for benzene, toluene, *p*-, *m*- and *o*-xylene at 3288 nm was 4.3, 7.4, 11.0, 12.5 and 6.2 ppb, respectively. In 2018, Tomberg et al. demonstrated the ability of CEPAS to reach a sub-ppt level sensitivity in HF gas detection, by using a high optical power of 950 mW [42]. The high stability of the experimental setup allowed long averaging times up to 32 min and the MDL reached 0.65 ppt. In 2019, the same team combined CEPAS with an optical power build-up cavity, which enhanced the photoacoustic signal by a factor of ~100 [43]. The optical cavity consisted of highly reflective mirrors that repeatedly reflect light so that the light travelled back and forth in the photoacoustic cavity many times. The achieved MDL was 24 ppt with a 100 s integration time and the NNEA was 1.75×10^{-12} $cm^{-1}WHz^{-1/2}$ for C_2H_2 detection. This is the best reported NNEA of PAS so far, to our knowledge.

(2) Fabry-Perot interference

Michelson interferometer has high sensitivity and good stability, but the bulky volume and high cost limit its application in some specific fields. CEPAS based on Fabry-Perot interferometer is relatively compact [50–62]. A Fabry-Perot cavity is formed between the end facet of the fiber and the free end of the cantilever. Light propagates along the lead-in fiber, then partial light is reflected by the end facet of the fiber and the rest is reflected by the surface of the cantilever. The optical path of the two reflected beams are different so the interference signal is generated. The length of the Fabry-Perot cavity varies along with the vibration of the cantilever, which can be calculated according to its output light intensity or phase detected by a demodulation unit, and then the displacement of cantilever can be obtained. In 2013, Wei et al. firstly combined CEPAS with a Fabry-Perot interferometer [50]. A MEMS cantilever was fabricated by surface micro-machining technology and the interference signal was detected by a photodiode. Water vapor was chosen as the target sample gas and the NNEA was 1.08×10^{-7} $cm^{-1}WHz^{-1/2}$. Chen et al. reported a stainless steel Fabry-Perot cantilever fabricated by laser cut in 2018 [51–53], as shown in Fig. 3. The resonant frequency of the cantilever was 1.4 kHz and the Q factor was 28.6. Then they introduced another demodulation method by a high-speed white-light interferometer, whose spectral sampling was synchronously triggered by a phased locked signal to maintain the working point of the probe laser at the quadrature point (Q-point) [54]. The gas detection limit of C_2H_2 was ~71 ppt with an averaging time of 200 s and the NNEA was 1.1×10^{-9} $cm^{-1}WHz^{-1/2}$. The sensitivity can be further improved by combining the acoustic resonance of the tube with the mechanical resonance of the cantilever [57]. By changing the temperature of the system, Chen et al. made the resonant frequency of the cantilever microphone and the acoustic resonant tube equal. The Q factor of the double resonance system increased from 28.6 to 46.3. The gas detection limit of C_2H_2 reached 27 ppt with an averaging time of 200 s and the NNEA was 4.2×10^{-10} $cm^{-1}WHz^{-1/2}$.

(3) Light intensity detection

Different from the optical interference detection method, the intensity detection method is more direct and its system is simpler. Usually, a split detector, like quadrant photodiode, is used to detect the displacement of the cantilever. A probe laser illuminates the cantilever surface and then the laser beam is reflected to the split detector. The difference between the intensity on each section of the split detector yields a photocurrent proportional to the displacement of the cantilever.

Westergaard et al. reported a CEPAS based on a stripped single-mode fiber [63]. The fiber itself was used as a cantilever and the emergent light of the fiber was detected by a split detector. Utilizing a 455 nm LED as the gas detection source, the MDL of NO_2 was approximately 50 ppm. Rakovsky et al. presented a mica cantilever to detect highly corrosive gasses like HCl and HBr, as shown in Fig. 4 [64]. Acoustic pressure was generated by a pulsed 10 Hz infrared optical parametric oscillator/-amplifier (OPO/OPA) laser and then acted on the mica cantilever. The split-photodiode detector was realized using a monolithic quadrature photodiode unit. Two adjacent photodiode segments were used for the probe beam position detection, which were placed ≈ 10 cm from the cantilever surface. Suchánek et al. compared a mica circular cantilever, a mica rectangular cantilever, and a multilayer graphene (MLG) cantilever for CEPAS [65,66]. A He-Ne laser together with a four-quadrant detector were used to detect the movement of the cantilevers. The MDL of methanol vapors were 0.8, 1.8, 0.9 ppm for these three kinds of

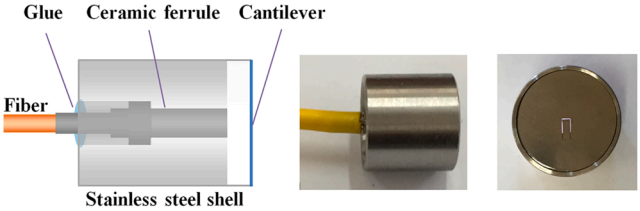

Fig. 3. Schematic structure and images of a Fabry-Perot cantilever [52].

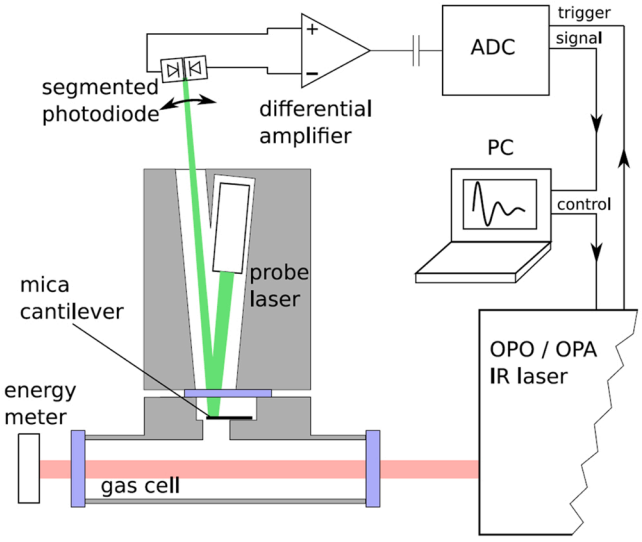

Fig. 4. Schematics of a CEPAS system based on light intensity detection [64].

cantilevers, respectively.

Different from the above reports, Li et al. introduced a compact all-optical cantilever sensor without using a split photodiode detector [67]. The device, consisting of a silicon cantilever, a rib waveguide and two optical fibers, was constructed based on a silicon-on-insulator (SOI) substrate, as shown in Fig. 5. The detection light from the input fiber was coupled into the waveguide and then collected by a photodetector at the end of the output fiber. The transmitted light intensity will variate as the cantilever vibrates. The minimum detectable acoustic pressure of the cantilever sensor was experimentally demonstrated as 35 nPa/Hz$^{1/2}$ at the resonant frequency (150 Hz).

3.2. CEPAS based on Non-optical detection

Although optical detection methods provide very good sensing performances for CEPAS, their potential integration in a compact system is limited by the complicated optical system. Silicon cantilevers fabricated by MEMS technology can be integrated with complex CMOS electronics. Recent progress in laser sources shows that mid-infrared lasers for gas

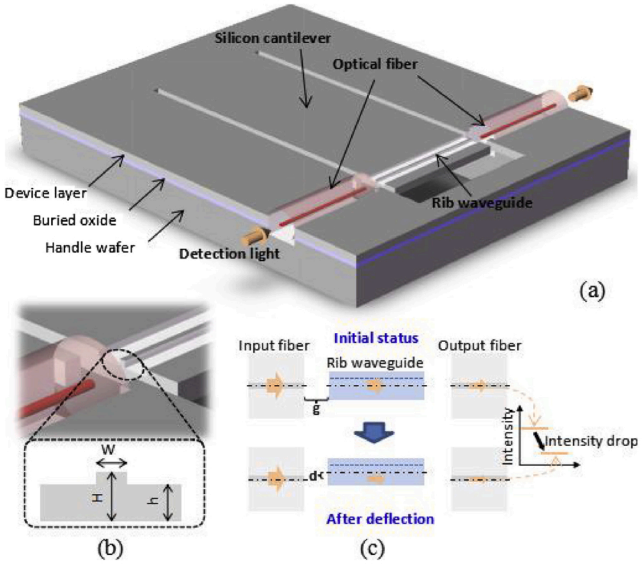

Fig. 5. Schematic and of working principle of the cantilever with an integrated rib waveguide [67].

spectroscopy can be integrated on silicon [68,69]. In the future, it is possible to integrate a silicon resonator, a semiconductor laser, and signal processing circuits on the same chip. Therefore, it is important to study non-optical on-chip displacement detection methods. The most common transduction methods in MEMS are based on capacitive, piezoelectric, and piezoresistive effects and all of them have been implemented in CEPAS.

(1) Capacitive detection

If a cantilever is placed close to a parallel electrode, the displacement of the cantilever will cause a capacitance change. In a MEMS sensor fabricated by silicon-on-insulator (SOI) technology, the buried oxide is often used as a sacrificial layer to define the separation between cantilever and counter electrode. No additional layer (like electrodes and functional materials) needs to be added on the cantilever, which maintain the cantilevers' mechanical performance. In capacitive transduction, the electric signal is inversely proportional to the distance between the electrodes so the electrodes gap is usually a few micrometers. However, small gap will cause great viscous damping called squeeze film effect [70]. In CEPAS, capacitive cantilever should be carefully designed to achieve a good performance [71]. Therefore, in the following, some capacitive resonators that are not in the traditional cantilever form will be introduced.

Chamassi et al. implemented a cantilever on a SOI wafer and designed a 8-shaped resonator in order to increase the Q factor and the overlapping area with the acoustic wave excitations [72]. The cantilever and the 8-shaped resonator presented a resonance frequency of 52 kHz and 14 kHz and a quality factor of 4 and 149, respectively. The signal ratio of the 8-shaped resonator was around 15 times of the simple cantilever. The 8-shaped resonator was used to detect C_2H_4 and achieves an MDL of 45 ppmv and a NNEA of 2.155×10^{-5} cm^{-1}WHz$^{-1/2}$.

Trzpil et al. introduced a H-shaped silicon resonator with capacitive detection to decrease the squeeze film of the traditional cantilever, as shown in Fig. 6 [73]. The H-shaped resonator was divided into several parts: zone 1 was designed to maximize the photoacoustic energy collection, zones 2 was designed to maximize the capacitive transduction, zone 3 connected zone 1 and zone 2, zone 4 held all the structure. They added a hole below zone 1 to decrease the viscous damping and particularly avoid the squeeze film effect. Zone 2 was composed of several long and thin clamped-free cantilevers and the distance between the zone 2 and the substrate was 3 μm to achieve high capacitance detection sensitivity. The resonant frequency of the H-shaped resonator was 44.79 kHz and the quality factor came up to 266. The performance of the H-shaped resonator was compared with a QEPAS system (32.7 kHz, Q=13000) in the detection of CH_4. The NNEA of H-shaped resonator and QEPAS was 5.5×10^{-7} cm^{-1}WHz$^{-1/2}$ and 1.3×10^{-7} cm^{-1}WHz$^{-1/2}$, respectively. Although the silicon-based micro resonator is in its early stage of development, its performances are comparable to the on-beam QEPAS performances.

(2) Piezoelectric detection

Piezoelectricity has been widely used for both cantilever actuation and detection. Some piezoelectric materials like ceramics, single crystals and polymers can translate the deformation of cantilever to voltage variation. One advantage of piezoelectric detection method is that no additional power is needed for the sensing. With the development of piezoelectric materials, different piezoelectric sensors have been used in CEPAS [74].

In 2004, Ledermann et al. reported a Pb(Zr_x, Ti_{1-x})O_3 (PZT) cantilever for CO_2 detection [75]. Fig. 7 shows the structure and principle of the PZT cantilever. The piezoelectric PZT films were deposited on the silicon structure. The area of the cantilever was 2×2 mm^2 and the thickness was 10–15 μm. Narrow slits of 3–5 μm around the cantilever were designed to improve the sensitivity at low frequencies. The

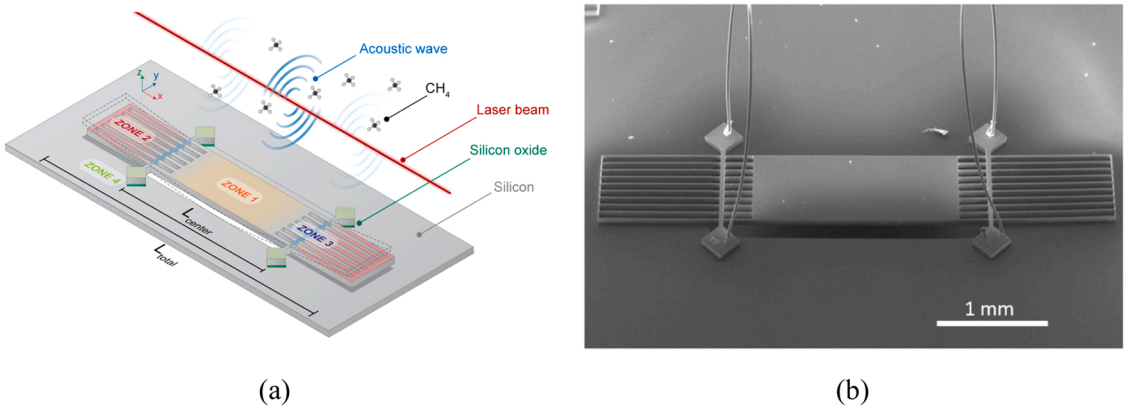

Fig. 6. The structure of the H-shaped capacitive silicon resonator [73]. (a) Scheme of the resonator under photoacoustic excitation. (b) Scanning electron microscopy picture.

acoustic response of the microphone reached 170 mV Pa^{-1} and the noise level was 150 μV $Hz^{-1/2}$. Concentration of CO_2 down to 330 ppm was measured and the acoustic detection limit was estimated to be 1.6 mPa $Hz^{-1/2}$ at a modulation frequency of 20 Hz.

In 2018, Liu et al. introduced a novel sensing approach based on low cost polyvinylidene fluoride (PVDF) film for PAS [76]. PVDF film possesses good flexibility, crash worthiness, high-voltage resistance, water resistance, and chemical stability, which may have potential applications under harsh or specific environmental conditions. A miniature acoustic resonator (AR) with a thin hole in the middle was designed for coupling acoustic wave to the PVDF film (Measurement Specialties, 0.2 mm thick) for PA signal detection, as shown in Fig. 8. The signal produced from the PVDF film was amplified by a preamplifier (EG&G, Model 5113) with a gain of 1000. Second harmonic signal of ambient H_2O vapor absorption was measured using the developed PVDF-PAS and the modulation frequency was 2963 Hz. The MDL was 5 ppmv with a lock in amplifier time constant of 70 s. The NNEA was calculated as 2.4×10^{-7} $cm^{-1}WHz^{-1/2}$, taking into account the laser power and bandwidth.

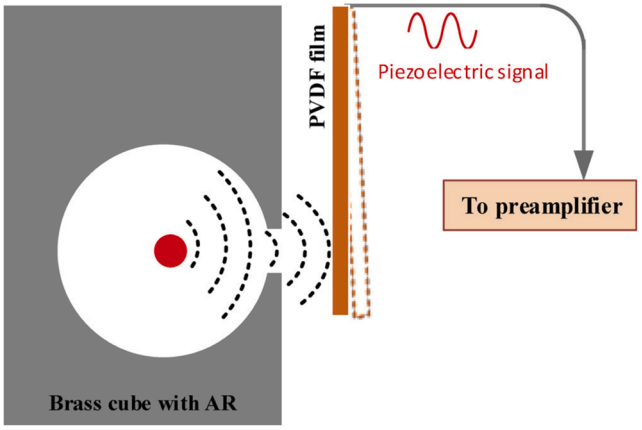

Fig. 8. Schematic of the PAS based on the PVDF cantilever [76].

(3) Piezoresistive detection

Piezoresistive cantilevers use the resistance change of materials under stress to measure the deformation of cantilevers. The piezoresistive cantilevers can be integrated with CMOS for signal processing and integrated for array-based operation easily.

Lhermet et al. reported a micro photoacoustic cell with integrated piezoresistive cantilever microphone [77–79]. This is the third-generation device of miniature photoacoustic components at CEA-LETI (a laboratory in French Atomic Energy and Alternative Energy Commission). Fig. 9 shows the structure of the device and the readout principle. The MEMS cell consisted of a photoacoustic chamber and a closed expansion volume, separated by a channel where a cantilever beam was placed. The cantilever beam would rotate around a flexible hinge when the modulated laser established a pressure fluctuation in the

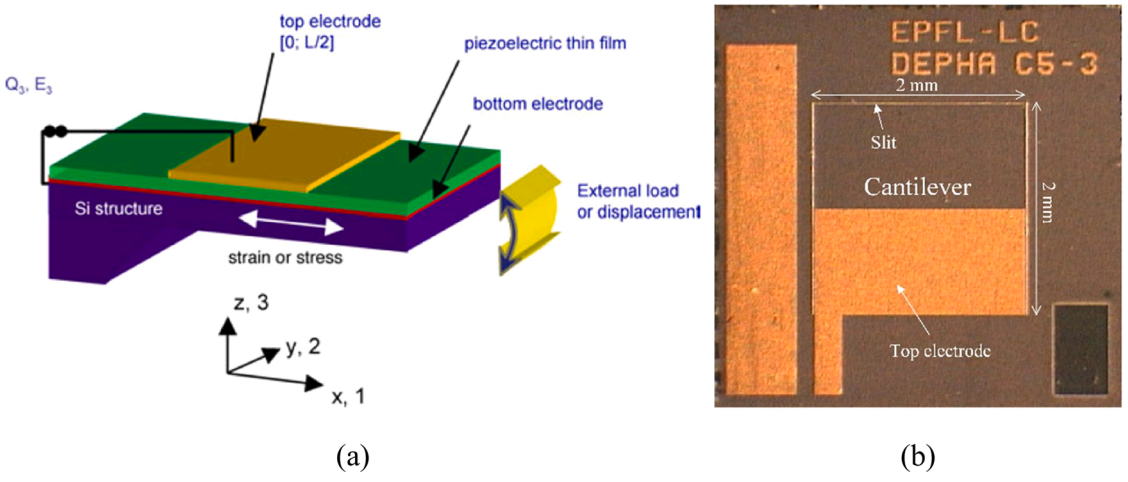

Fig. 7. The structure of the PZT cantilever [75]. (a) Piezoelectric effect in MEMS cantilever. (b) Optical image of a 2 × 2 mm^2 cantilever.

photoacoustic chamber. This cantilever motion produced a significant longitudinal stress inside two suspended piezoresistive p-doped Si nano-gauges and was thus transduced into resistance variations. The cantilever was 3.9 μm high, 750 μm long and showed a resonant frequency of 6.5 kHz in the cell. Measurements of CH_4 and CO_2 were performed to assess the gas-sensing capabilities of the device. The MDL for CH_4 was estimated at 1.4 ppm (54 s integration time) and the NNEA was 5×10^{-8} $cm^{-1}WHz^{-1/2}$, using an interband cascade laser (ICL) tuned to the 2979 cm^{-1} absorption line. The MDL for CO_2 was estimated to be 900 ppb (1 s integration time) and the NNEA was 3×10^{-7} $cm^{-1}WHz^{-1/2}$, using an QCL tuned to the 2302 cm^{-1} absorption line. The photoacoustic sensor was built by stacking two 200 mm wafers and the overall area was 5.5 mm × 5.5 mm, which showed a very high integration.

A transistor can be directly embedded at the base of the piezoresistive cantilever to transduce its deflection and can dramatically improve its sensitivity [80,81]. Talukdar et al. reported an AlGaN/GaN heterojunction field effect transistor (HFET) embedded GaN microcantilever for PAS, as shown in Fig. 10 [82,83]. They used commercial wafers with III-V nitride epitaxial layers on Si (111) substrate and an AlGaN/GaN heterojunction field effect transistor (HFET) as a piezoresistive deflection sensor, which was called 'piezotransistive' sensor in their publication. The strong piezoelectric property of HFET can cause large variation in 2-dimensional electron gas (2DEG) at the interface with applied mechanical strain. The resonant frequency of the cantilever was ~45 kHz and the Q factor was ~200 in the air. The microcantilever can be used as air based ultrasonic sensor [82]. The noise limited pressure measurement resolution of the cantilever at resonant frequency was calculated as 1.96 μPa for 1 Hz bandwidth. The microcantilever can also be used as a surface wave detector, which is capable of measuring surface wave amplitudes in the tens of femtometer range [83]. Finally, two different analytes, polystyrene (PS) and research development explosive (RDX), were tested using a surface-based photoacoustic spectroscopy technique. These analytes were deposited near the base of a microcantilever and a laser was focused on them and pulsed at the resonance frequency of the microcantilever. The absorption spectrums of both the analytes (300 ng) were detected, which showed good SNR and closely matched the absorption peaks reported earlier.

4. Conclusions

This review compares different displacement detection techniques for CEPAS systems, which can be divided into optical detection and non-optical detection. The optical detection methods mainly include Michelson interference, Fabry-Perot interference and light intensity detection and the non-optical detection methods include capacitive,

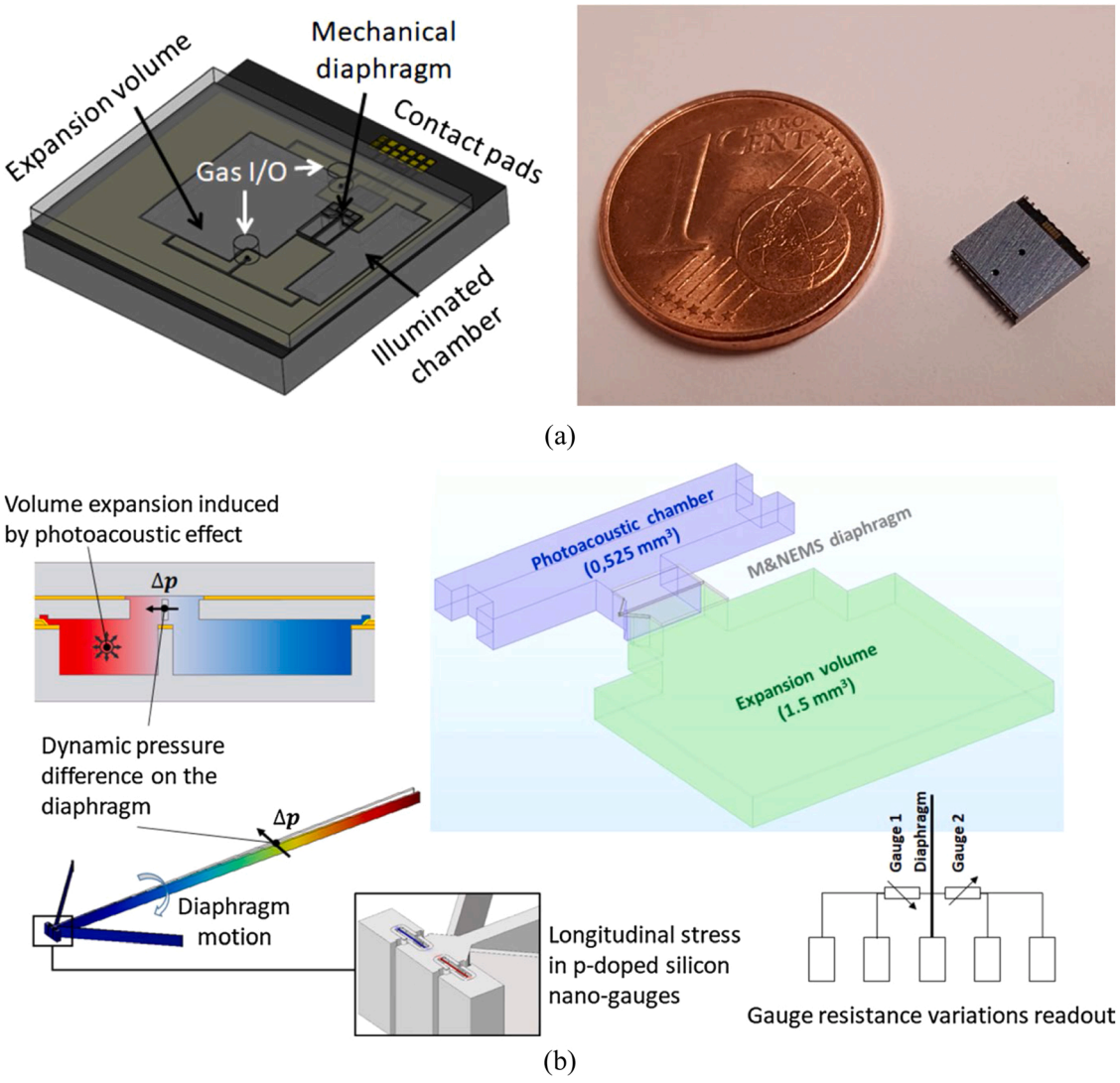

Fig. 9. The photoacoustic sensor of CEA-LETI [79]. (a)Structure of the silicon-integrated sensor (left) and photo of the manufactured chip (right). (b) Principle of the micro PAS system with a piezoresistive readout cantilever.

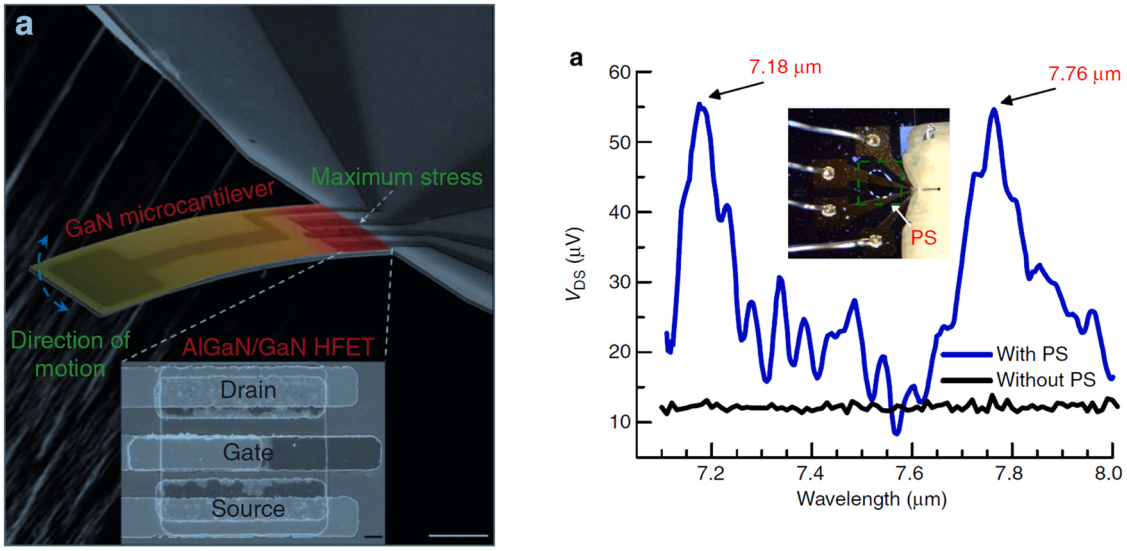

Fig. 10. AlGaN/GaN HFET-embedded GaN microcantilever. (a) SEM image of the structure. (b) Photoacoustic spectroscopy of analytes (PS) with HFET readout [83].

piezoelectric and piezoresistive detection. The MDL and the NNEA of different methods are summarized in Table 1.

Michelson interference method achieves a best MDL of 0.65 ppt and a best NNEA of 1.75×10^{-12} $cm^{-1}WHz^{-1/2}$, which shows the first-class performance among all of the detection techniques in CEPAS. However, the use of complex Michelson interferometer results in high cost and bulky volume. CEPAS based on Fabry-Perot interference method is relatively compact and the MDL can still maintain an outstanding level of dozens of ppt. A disadvantage of Fabry-Perot interference is that the probe laser needs to work at the quadrature point, which is easily drifted with the ambient temperature. Different from the optical interference detection method, the light intensity detection method is more direct and the optical system is simpler. But the MDL of CEPAS based on light intensity detection can only reach ppm level nowadays, because the light intensity is easily affected by the laser power fluctuation and the sensing system stability. Capacitive detection is a common readout method in MEMS sensors but the capacitive cantilevers for CEPAS suffer from large squeeze film damping because of the narrow electrodes gap. This disadvantage limits the sensitivity of the capacitive detection, which results in an MDL of only dozens of ppm. Piezoelectric detection has the advantages of self-power supply and low cost. With the development of piezoelectric materials, the sensitivity of piezoelectric cantilevers is also improved. The sensitive structure of piezoresistive cantilevers usually use semiconductor materials such as silicon, which is attracting for integration. A transistor can be directly embedded at the base of the piezoresistive cantilever to transduce its deflection and can dramatically improve its sensitivity. These non-optical detection methods show a best NNEA level of $10^{-7} \sim 10^{-8}$ $cm^{-1}WHz^{-1/2}$, which is 2–3 orders of magnitude lower than the common optical interference methods.

Optical detection methods provide very good sensing performances for CEPAS. The ppt level detection limit is ideal for precise trace gas measurements, which can be applied in metrology, atmospheric monitoring, industrial process detection, hazardous substances detection, breath diagnosis, etc. The sensitivity of optical-based CEPAS could be further improved by increasing the optical path and the optical power in the photoacoustic cell, for example, using an optical cavity with reflecting mirrors. CEPAS based on non-optical detection has the

Table 1
Comparison of CEPAS with different displacement detection methods.

Ref	Method	Target gas	Laser type	Wavelength (nm)	Power (mW)	MDL (at a specific averaging time)	NNEA ($cm^{-1}WHz^{-1/2}$)
[30]	MI	CO_2	DFB	1572	30	0.3 ppm (100 s)	1.7×10^{-10}
[33]	MI	CO	DFB	1568	2.93	249.6 ppm (2.62 s)	3.4×10^{-9}
		C_2H_2		1534	1.71	1.5 ppm (2.62 s)	3.6×10^{-9}
		CH_4		1618	0.81	293.7 ppm (2.62 s)	1.4×10^{-9}
[36]	MI	HCN	OPO	3002	500	190 ppt (1 s)	1.8×10^{-9}
		CH_4		3270	600	65 ppt (30 s)	/
[42]	MI	HF	OPO	2476	950	2.5 ppt (15 s) or 0.65 ppt (32 min)	5.19×10^{-10}
[43]	MI	C_2H_2	DFB	1532	7.5	24 ppt (100 s)	1.75×10^{-12}
[50]	FPI	H_2O	DFB	1392	7.8	/	1.08×10^{-7}
[54]	FPI	C_2H_2	DFB with DEFA	1533	1000	71 ppt (200 s)	1.1×10^{-9}
[57]	FPI	C_2H_2	DFB with DEFA	1533	1000	27 ppt (200 s)	4.2×10^{-10}
[66]	Light intensity	CH_3COCH_3	CO_2 laser	9240	170	24.8 ppm	/
		CH_3COOH		10,240	~	0.54 ppm	
		CH_3OH		9500	1000	0.8 ppm	
[72]	Capacitive	C_2H_4	QCL	10,922	4	45 ppm (21 s)	2.155×10^{-5}
		CH_4	DFB	1653	6	242 ppm (10 min)	4.664×10^{-5}
[73]	Capacitive	CH_4	DFB	2325	3.86	264 ppm (10 s)	5.5×10^{-7}
[76]	Piezoelectric	H_2O	DFB	1395	9	5 ppm (70 s)	2.4×10^{-7}
[77]	Piezoresistive	CO_2	QCL	4343	4.88	0.9 ppm (1 s)	3×10^{-7}
[78]	Piezoresistive	CH_4	ICL	3357	4	1.4 ppm (54 s)	5×10^{-8}

potential to integrate the entire system on a single chip and to be mass-produced. The tiny and cheap CEPAS sensors can be used in smart systems and portable detection devices on a large scale. However, as the sensor volume decreases, the influence of the viscous and thermal surface losses effects becomes prominent. The photoacoustic cell and the cantilever should be designed carefully to balance miniaturization with high performance. In addition, the high performance on-chip laser source and its integration with photoacoustic system are still challenging.

Finally, if the CEPAS sensors are used for continuous monitoring over long periods of time, the stability of the sensor system should be studied. The use of mechanical cantilever makes the sensor more susceptible to environmental factors such as temperature and air pressure. Especially when both the cantilever and the photoacoustic cell work in resonant state, the frequency drift and amplitude drift of the whole system should be suppressed or compensated to improve the long-term stability of CEPAS.

Declaration of Competing Interest

The authors declare that they have no known competing financial interests or personal relationships that could have appeared to influence the work reported in this paper.

Data Availability

No data was used for the research described in the article.

Acknowledgments

We would like to acknowledge the financial support from Center-initiated Research Project of Zhejiang Lab (Grant No. K2022MG0AL08), Zhejiang Provincial Natural Science Foundation (Grant No. LQ22D050003) and National Natural Science Foundation of China (Grant No. 62205299).

References

[1] Y. Adiguzel, H. Kulah, Breath sensors for lung cancer diagnosis, Biosens. Bioelectron. 65 (2015) 121–138.
[2] R.C. Sharma, S. Kumar, S. Gautam, S. Gupta, H.B. Srivastava, Photoacoustic sensor for trace detection of post-blast explosive and hazardous molecules, Sens. Actuators B Chem. 243 (2017) 59–63.
[3] S. Zhou, D. Iannuzzi, Immersion photoacoustic spectrometer (iPAS) for arcing fault detection in power transformers, Opt. Lett. 44 (15) (2019) 3741–3744.
[4] J. Hodgkinson, R.P. Tatam, Optical gas sensing: a review, Meas. Sci. Technol. 24 (1) (2013).
[5] S. Lin, J. Chang, J.C. Sun, P. Xu, Improvement of the detection sensitivity for tunable diode laser absorption spectroscopy, A Rev., Front. Phys. 10 (2022).
[6] S. Maithani, M. Pradhan, Cavity ring-down spectroscopy and its applications to environmental, chemical and biomedical systems, J. Chem. Sci. 132 (1) (2020).
[7] A. Miklos, P. Hess, Z. Bozoki, Application of acoustic resonators in photoacoustic trace gas analysis and metrology, Rev. Sci. Instrum. 72 (4) (2001) 1937–1955.
[8] E.L. Holthoff, P.M. Pellegrino, Development of photoacoustic sensing platforms at the Army Research Laboratory, Appl. Opt. 56 (3) (2017) B74–B84.
[9] C. Haisch, Photoacoustic spectroscopy for analytical measurements, Meas. Sci. Technol. 23 (1) (2012).
[10] M.J. Navas, A.M. Jimenez, A.G. Asuero, Human biomarkers in breath by photoacoustic spectroscopy, Clin. Chim. Acta 413 (15–16) (2012) 1171–1178.
[11] J.S. Li, W.D. Chen, B.L. Yu, Recent progress on infrared photoacoustic spectroscopy techniques, Appl. Spectrosc. Rev. 46 (6) (2011) 440–471.
[12] D.C. Dumitras, M. Petrus, A.M. Bratu, C. Popa, Applications of near infrared photoacoustic spectroscopy for analysis of human respiration: a review, Molecules 25 (7) (2020).
[13] T.H. Yang, W.G. Chen, P.Y. Wang, A review of all-optical photoacoustic spectroscopy as a gas sensing method, Appl. Spectrosc. Rev. 56 (2) (2021) 143–170.
[14] H.P. Wu, L. Dong, H.D. Zheng, Y.J. Yu, W.G. Ma, L. Zhang, W.B. Yin, L.T. Xiao, S. T. Jia, F.K. Tittel, Beat frequency quartz-enhanced photoacoustic spectroscopy for fast and calibration-free continuous trace-gas monitoring, Nat. Commun. 8 (2017) 15331.
[15] P. Patimisco, G. Scamarcio, F.K. Tittel, V. Spagnolo, Quartz-enhanced photoacoustic spectroscopy: a review, Sensors 14 (4) (2014) 6165–6206.
[16] P. Patimisco, A. Sampaolo, L. Dong, F.K. Tittel, V. Spagnolo, Recent advances in quartz enhanced photoacoustic sensing, Appl. Phys. Rev. 5 (1) (2018), 011106.
[17] P. Patimisco, S. Borri, I. Galli, D. Mazzotti, G. Giusfredi, N. Akikusa, M. Yamanishi, G. Scamarcio, P. De Natale, V. Spagnolo, High finesse optical cavity coupled with a quartz-enhanced photoacoustic spectroscopic sensor, Analyst 140 (3) (2015) 736–743.
[18] Y.F. Ma, Review of recent advances in QEPAS-based trace gas sensing, Appl. Sci. 8 (10) (2018).
[19] H.D. Zheng, L. Dong, A. Sampaolo, H.P. Wu, P. Patimisco, X.K. Yin, W.G. Ma, L. Zhang, W.B. Yin, V. Spagnolo, S.T. Jia, F.K. Tittel, Single-tube on-beam quartz-enhanced photoacoustic spectroscopy, Opt. Lett. 41 (5) (2016) 978–981.
[20] G. Wysocki, A.A. Kosterev, F.K. Tittel, Influence of molecular relaxation dynamics on quartz-enhanced photoacoustic detection of CO_2 at lambda=2 mu m, Appl. Phys. B Lasers Opt. 85 (2–3) (2006) 301–306.
[21] A.A. Kosterev, Y.A. Bakhirkin, F.K. Tittel, Ultrasensitive gas detection by quartz-enhanced photoacoustic spectroscopy in the fundamental molecular absorption bands region, Appl. Phys. B Lasers Opt. 80 (1) (2005) 133–138.
[22] R. Lewicki, G. Wysocki, A.A. Kosterev, F.K. Tittel, Carbon dioxide and ammonia detection using 2 mu m diode laser based quartz-enhanced photoacoustic spectroscopy, Appl. Phys. B Lasers Opt. 87 (1) (2007) 157–162.
[23] K.S. Zhang, W.H. Ou, X.Q. Jiang, F. Long, M.Z. Hu, Calculation of vibrational relaxation times in multi-component excitable gases, J. Korean Phys. Soc. 65 (7) (2014) 1028–1035.
[24] S.L. Firebaugh, K.F. Jensen, M.A. Schmidt, Miniaturization and integration of photoacoustic detection, J. Appl. Phys. 92 (3) (2002) 1555–1563.
[25] Q. Wang, J. Chang, F.P. Wang, W. Wei, Recovery of pure wavelength modulation second harmonic signal waveforms in distributed feedback diode laser-based photoacoustic spectroscopy, Sens. Actuators A Phys. 245 (2016) 54–62.
[26] P. Werle, R. Mücke, F. Slemr, The limits of signal averaging in atmospheric trace-gas monitoring by tunable diode-laser absorption spectroscopy (TDLAS), Appl. Phys. B 57 (2) (1993) 131–139.
[27] L.S. Rothman, D. Jacquemart, A. Barbe, D. Chris Benner, M. Birk, L.R. Brown, M. R. Carleer, C. Chackerian, K. Chance, L.H. Coudert, V. Dana, V.M. Devi, J.M. Flaud, R.R. Gamache, A. Goldman, J.M. Hartmann, K.W. Jucks, A.G. Maki, J.Y. Mandin, S. T. Massie, J. Orphal, A. Perrin, C.P. Rinsland, M.A.H. Smith, J. Tennyson, R. N. Tolchenov, R.A. Toth, J. Vander Auwera, P. Varanasi, G. Wagner, The HITRAN 2004 molecular spectroscopic database, J. Quant. Spectrosc. Radiat. Transf. 96 (2) (2005) 139–204.
[28] K. Wilcken, J. Kauppinen, Optimization of a microphone for photoacoustic spectroscopy, Appl. Spectrosc. 57 (9) (2003) 1087–1092.
[29] T. Kuusela, J. Kauppinen, Photoacoustic gas analysis using interferometric cantilever microphone, APPL SPECTROSC REV 42 (2007) 443–474.
[30] V. Koskinen, J. Fonsen, K. Roth, J. Kauppinen, Cantilever enhanced photoacoustic detection of carbon dioxide using a tunable diode laser source, Appl. Phys. B 86 (3) (2007) 451–454.
[31] V. Koskinen, J. Fonsen, K. Roth, J. Kauppinen, Progress in cantilever enhanced photoacoustic spectroscopy, Vib. Spectrosc. 48 (1) (2008) 16–21.
[32] I. Kauppinen, A. Branders, J. Uotila, J. Kauppinen, T. Kuusela, G. Ltd, Sensitive and fast gas sensor for wide variety of applications based on novel differential infrared photoacoustic principle, Tm. Tech. Mess. 79 (2012).
[33] E.D. McNaghten, K.A. Grant, A.M. Parkes, P.A. Martin, Simultaneous detection of trace gases using multiplexed tunable diode lasers and a photoacoustic cell containing a cantilever microphone, Appl. Phys. B Lasers Opt. 107 (3) (2012) 861–871.
[34] C.B. Hirschmann, J. Lehtinen, J. Uotila, S. Ojala, R.L. Keiski, Sub-ppb detection of formaldehyde with cantilever enhanced photoacoustic spectroscopy using quantum cascade laser source, Appl. Phys. B Lasers Opt. 111 (4) (2013) 603–610.
[35] C.B. Hirschmann, S. Sinisalo, J. Uotila, S. Ojala, R.L. Keiski, Trace gas detection of benzene, toluene, p-, m- and o-xylene with a compact measurement system using cantilever enhanced photoacoustic spectroscopy and optical parametric oscillator, Vib. Spectrosc. 68 (2013) 170–176.
[36] J. Peltola, M. Vainio, T. Hieta, J. Uotila, S. Sinisalo, M. Metsala, M. Siltanen, L. Halonen, High sensitivity trace gas detection by cantilever-enhanced photoacoustic spectroscopy using a mid-infrared continuous-wave optical parametric oscillator, Opt. Express 21 (8) (2013) 10240–10250.
[37] P. Sievila, N. Chekurov, J. Raittila, I. Tittonen, Sensitivity-improved silicon cantilever microphone for acousto-optical detection, Sens. Actuators a Phys. 190 (2013) 90–95.
[38] J. Lehtinen, T. Kuusela, Broadly tunable quantum cascade laser in cantilever-enhanced photoacoustic infrared spectroscopy of solids, Appl. Phys. B Lasers Opt. 115 (3) (2014) 413–418.
[39] H. Moser, B. Lendl, Cantilever-enhanced photoacoustic detection of hydrogen sulfide (H2S) using NIR telecom laser sources near 1.6 mu m, Appl. Phys. B Lasers Opt. 122 (4) (2016).
[40] X.X. Zhang, Z. Cheng, X. Li, Cantilever enhanced photoacoustic spectrometry: quantitative analysis of the trace H2S produced by SF6 decomposition, Infrared Phys. Technol. 78 (2016) 31–39.
[41] M. Dostal, J. Suchanek, V. Valek, Z. Blatonova, V. Nevrly, P. Bitala, P. Kubat, Z. Zelinger, Cantilever-enhanced photoacoustic detection and infrared spectroscopy of trace species produced by biomass burning, Energy Fuels 32 (10) (2018) 10163–10168.
[42] T. Tomberg, M. Vainio, T. Hieta, L. Halonen, Sub-parts-per-trillion level sensitivity in trace gas detection by cantilever-enhanced photo-acoustic spectroscopy, Sci. Rep. 8 (1) (2018) 1848.
[43] T. Tomberg, T. Hieta, M. Vainio, L. Halonen, Cavity-enhanced cantilever-enhanced photo-acoustic spectroscopy, Analyst 144 (7) (2019) 2291–2296.

[44] H.T. Cheng, X.X. Zhang, C. Bian, J. Cheng, Z.W. Chen, Y. Zhang, J. Tang, S. Xiao, Photoacoustic spectroscopy: trace CO detection by using 10 mW near-infrared laser and cantilever beam, AIP Adv. 10 (10) (2020).
[45] J. Karhu, H. Philip, A. Baranov, R. Teissier, T. Hieta, Sub-ppb detection of benzene using cantilever-enhanced photoacoustic spectroscopy with a long-wavelength infrared quantum cascade laser, Opt. Lett. 45 (21) (2020) 5962–5965.
[46] H.T. Cheng, J. Tang, X.X. Zhang, Y. Li, J.Y. Hu, Y. Zhang, S.Y. Mao, S. Xiao, Simultaneous detection of C2H2 and CO based on cantilever-enhanced photoacoustic spectroscopy, IEEE Trans. Instrum. Meas. 70 (2021).
[47] J. Karhu, T. Hieta, F. Manoocheri, M. Vainio, E. Ikonen, LED-based photoacoustic NO2 sensor with a sub-ppb detection limit, ACS Sens 6 (9) (2021) 3303–3307.
[48] J. Karhu, J. Kuula, A. Virkkula, H. Timonen, M. Vainio, T. Hieta, Cantilever-enhanced photoacoustic measurement of light-absorbing aerosols, Aerosol Sci. Technol. 56 (1) (2021) 92–100.
[49] F.X. Ma, Z.H. Liao, Y. Zhao, Z.J. Qiu, L.J. Wan, K. Li, G.Q. Zhang, Detection of trace C2H2 in N-2 buffer gas with cantilever-enhanced photoacoustic spectrometer, Optik 232 (2021).
[50] W. Wei, Y. Zhu, C. Lin, L. Tian, Z.W. Xu, J.P. Nong, All-optical cantilever-enhanced photoacoustic spectroscopy in the open environment, Int. J. Thermophys. 36 (5–6) (2015) 1116–1122.
[51] K. Chen, Z.F. Gong, M. Guo, S.C. Yu, C. Qu, X.L. Zhou, Q.X. Yu, Fiber-optic Fabry-Perot interferometer based high sensitive cantilever microphone, Sens. Actuators a Phys. 279 (2018) 107–112.
[52] K. Chen, Q.X. Yu, Z.F. Gong, M. Guo, C. Qu, Ultra-high sensitive fiber-optic Fabry-Perot cantilever enhanced resonant photoacoustic spectroscopy, Sens. Actuator B Chem. 268 (2018) 205–209.
[53] K. Chen, Z. Yu, Q. Yu, M. Guo, Z. Zhao, C. Qu, Z. Gong, Y. Yang, Fast demodulated white-light interferometry-based fiber-optic Fabry–Perot cantilever microphone, Opt. Lett. 43 (14) (2018) 3417–3420.
[54] K. Chen, Z.H. Yu, Z.F. Gong, Q.X. Yu, Lock-in white-light-interferometry-based all-optical photoacoustic spectrometer, Opt. Lett. 43 (20) (2018) 5038–5041.
[55] K. Chen, B. Zhang, S. Liu, Q.X. Yu, Parts-per-billion-level detection of hydrogen sulfide based on near-infrared all-optical photoacoustic spectroscopy, Sens. Actuator B Chem. 283 (2019) 1–5.
[56] M. Guo, K. Chen, Z.F. Gong, Q.X. Yu, Trace ammonia detection based on near-infrared fiber-optic cantilever-enhanced photoacoustic spectroscopy, photonic, Sensors 9 (4) (2019) 293–301.
[57] K. Chen, H. Deng, M. Guo, C. Luo, S. Liu, B. Zhang, F.X. Ma, F. Zhu, Z.F. Gong, W. Peng, Q.X. Yu, Tube-cantilever double resonance enhanced fiber-optic photoacoustic spectrometer, Opt. Laser Technol. (2020), 105894.
[58] T. Lauwers, A. Gliere, S. Basrour, An all-optical photoacoustic sensor for the detection of trace gas, Sensors 20 (14) (2020).
[59] K. Chen, M. Guo, B.L. Yang, F. Jin, G.Z. Wang, F.X. Ma, C.Y. Li, B. Zhang, H. Deng, Z.F. Gong, Highly sensitive optical fiber photoacoustic sensor for in situ detection of dissolved gas in oil, IEEE Trans. Instrum. Meas. 70 (2021).
[60] Y. Liu, F. Wang, J.Y. Liu, Quantification of proton radiation damage in polyimide aerogel by cantilever-enhanced photoacoustic spectroscopy, IEEE Trans. Instrum. Meas. 70 (2021).
[61] L. Fu, P. Lu, C. Sima, J. Zhao, Y. Pan, T. Li, X. Zhang, D. Liu, Small-volume highly-sensitive all-optical gas sensor using non-resonant photoacoustic spectroscopy with dual silicon cantilever optical microphones, Photoacoustics 27 (2022), 100382.
[62] M. Guo, K. Chen, C.X. Li, L. Xu, G.Y. Zhang, N. Wang, C.Y. Li, F.X. Ma, Z.F. Gong, Q.X. Yu, High-sensitivity silicon cantilever-enhanced photoacoustic spectroscopy analyzer with low gas consumption, Anal. Chem. 94 (2) (2022) 1151–1157.
[63] P.G. Westergaard, M. Lassen, All-optical detection of acoustic pressure waves with applications in photoacoustic spectroscopy, Appl. Opt. 55 (29) (2016) 8266–8270.
[64] J. Rakovský, O. Votava, A simple photoacoustic detector for highly corrosive gases, Rev. Sci. Instrum. 88 (1) (2017), 013103.
[65] J. Suchanek, M. Dostal, T. Vlasakova, P. Janda, M. Klusackova, P. Kubat, V. Nevrly, P. Bitala, S. Civis, Z. Zelinger, First application of multilayer graphene cantilever for laser photoacoustic detection, Measurement 101 (2017) 9–14.
[66] J. Suchánek, P. Janda, M. Dostál, A. Knížek, P. Kubát, P. Roupcová, P. Bitala, V. Nevrlý, Z. Zelinger, Photoacoustic spectroscopy with mica and graphene micro-mechanical levers for multicomponent analysis of acetic acid, acetone and methanol mixture, Microchem. J. 144 (2019) 203–208.
[67] W. Li, Z.H. Wang, C.H. Feng, Q. Li, H.B. Yu, High sensitivity all-optical acoustic pressure sensor based on resonant micro-opto-mechanical cantilever with integrated rib waveguide, Sens. Actuators a Phys. 285 (2019) 300–307.
[68] J.G. Coutard, M. Brun, M. Fournier, O. Lartigue, F. Fedeli, G. Maisons, J.M. Fedeli, S. Nicoletti, M. Carras, L. Duraffourg, Enabling low cost QCL by large scale fabrication on CMOS pilot line. SPIE OPTO, SPIE, 2020.
[69] M. Rio Calvo, L. Monge Bartolomé, M. Bahriz, G. Boissier, L. Cerutti, J.-B. Rodriguez, E. Tournié, Mid-infrared laser diodes epitaxially grown on on-axis (001) silicon, Optica 7 (4) (2020) 263–266.
[70] G. Wu, D. Xu, B. Xiong, Y. Ma, Y. Wang, E. Jing, Analysis of air damping in micromachined resonators, 2012 7th IEEE International Conference on Nano/Micro Engineered and Molecular Systems (NEMS), 2012, pp. 469–472.
[71] W. Trzpil, N. Maurin, R. Rousseau, D. Ayache, A. Vicet, M. Bahriz, Analytic optimization of cantilevers for photoacoustic gas sensor with capacitive transduction, Sensors 21 (4) (2021).
[72] K. Chamassi, W. Trzpil, R. Arinero, R. Rousseau, A. Vicet, M. Bahriz, Capacitive silicon micro-electromechanical resonator for enhanced photoacoustic spectroscopy, Appl. Phys. Lett. 115 (8) (2019), 081106.
[73] W. Trzpil, J. Charensol, D. Ayache, N. Maurin, R. Rousseau, A. Vicet, M. Bahriz, A silicon micromechanical resonator with capacitive transduction for enhanced photoacoustic spectroscopy, Sens. Actuators B Chem. (2021), 131070.
[74] H.H. Lv, H.J. Luo, H.D. Zheng, W.G. Zhu, J.B. Fang, J.H. Yu, F. Tittel, Z. Chen, Application of piezoelectric transducers in photoacoustic spectroscopy for trace gas analysis, Microw. Opt. Technol. Lett. 63 (8) (2021) 2040–2051.
[75] N. Ledermann, P. Muralt, J. Baborowski, M. Forster, J.P. Pellaux, Piezoelectric Pb(Zr-x,Ti1-x)O-3 thin film cantilever and bridge acoustic sensors for miniaturized photoacoustic gas detectors, J. Micromech. Micro 14 (12) (2004) 1650–1658.
[76] K. Liu, Y. Cao, G. Wang, W. Zhang, W. Chen, X. Gao, A novel photoacoustic spectroscopy gas sensor using a low cost polyvinylidene fluoride film, Sens. Actuators B Chem. 277 (2018) 571–575.
[77] H. Lhermet, T. Verdot, A. Teulle, A. Berthelot, A. Glière, B. Desloges, F. Souchon, M. Fournier, J.M. Fédéli, J.G. Coutard, Micro-Photoacoustic Cell with Integrated Microphone for Sub-Ppm Gas Sensing, 2019 20th International Conference on Solid-State Sensors, Actuators and Microsystems & Eurosensors XXXIII (TRANSDUCERS & EUROSENSORS XXXIII), 2019, pp. 68–71.
[78] J.G. Coutard, A. Berthelot, A. Glière, H. Lhermet, B. Scherer, T. Strahl, A. Teulle, T. Verdot, Micro PA detector: pushing the limits of mid IR photoacoustic spectroscopy integrated on silicon. SPIE OPTO, SPIE,, 2020.
[79] A. Glière, P. Barritault, A. Berthelot, C. Constancias, J.G. Coutard, B. Desloges, L. Duraffourg, J.M. Fedeli, M. Garcia, O. Lartigue, H. Lhermet, A. Marchant, J. Rouxel, J. Skubich, A. Teulle, T. Verdot, S. Nicoletti, Downsizing and silicon integration of photoacoustic gas cells, Int. J. Thermophys. 41 (2020) 16.
[80] G. Shekhawat, S.-H. Tark, V.P. Dravid, MOSFET-embedded microcantilevers for measuring deflection in biomolecular sensors, Science 311 (5767) (2006) 1592–1595.
[81] M. Qazi, N. Deroller, A. Talukdar, G. Koley, III-V Nitride based piezoresistive microcantilever for sensing applications, Appl. Phys. Lett. 99 (2011).
[82] A. Talukdar, M. Qazi, G. Koley, High frequency dynamic bending response of piezoresistive GaN microcantilevers, Appl. Phys. Lett. 101 (25) (2012).
[83] A. Talukdar, M.F. Khan, D. Lee, S. Kim, T. Thundat, G. Koley, Piezotransistive transduction of femtoscale displacement for photoacoustic spectroscopy, Nat. Commun. 6 (2015).

Yonggang Yin received the B.S. degree in mechanical engineering and automation from Tsinghua University, Beijing, China, in 2014, and the Ph.D. degree in instrumentation science and technology from Tsinghua University, in 2019. He is currently a research assistant professor in Zhejiang Lab, Hangzhou, China. His research interests include MEMS resonators, acoustic sensors and photoacoustic spectroscopy.

Danyang Ren have received the master's degree in State Key Laboratory of New Ceramics and Fine Processing, School of Materials Science and Engineering, Tsinghua University, Beijing, China, in 2019. She has received a bachelor's degree in materials science and engineering in 2016. After graduating in 2019, she went to Shenzhen BYD Lithium Battery Co., Ltd. as a senior development engineer, engaged in the research of active material materials and polymer separator materials for lithium batteries. From May 2020, she worked as an engineer in Zhejiang Lab, Hangzhou, China. And she mainly engaged in the research of composite piezoelectric materials and the manufacture of ultrasonic transducers.

Chiye Li is a research scientist at Center for Intelligent Sensing, Zhejiang Lab. He received his B.S. from University of Science and Technology of China in 2011, and his Ph.D. in Biomedical Engineering from Washington University in St. Louis in 2016. His research interests include biomedical optics and photoacoustic imaging.

Ruimin Chen (Member, IEEE) received the B.S. degree in biomedical engineering from the University of Electronics Science and Technology of China, Chengdu, China, in 2006, and the M.S. and Ph.D. degrees in biomedical engineering from the University of Southern California, Los Angeles, CA, USA, in 2008 and 2014, respectively. He was a Postdoctoral Research Associate and the Resource Manager with the NIH Ultrasonic Transducer Resource Center, Department of Biomedical Engineering, University of Southern California. He was also a Research Specialist with the USC Roski Eye Institute, University of Southern California. He was an Ultrasound Sensor Engineer with Masimo Corporation, Irvine, CA, USA. He is now an Associate Researcher with Zhejiang Laboratory, Hangzhou, China. His research interests include the design, modeling, and fabrication of high-frequency ultrasonic transducers and arrays for biomedical and industrial imaging applications.

Junhui Shi received his BSc in chemical physics from the University of Science and Technology of China. Then, he continued to study chemistry and received his PhD at Princeton University. He was working on theoretical chemical dynamics and experimental nuclear magnetic resonance spectroscopy. Afterward, he worked on photoacoustic imaging in the Department of Biomedical Engineering of Washington University in St. Louis, Missouri, and then in the Department of Medical Engineering of Caltech in Pasadena, California. Currently, he is a senior researcher at Zhejiang Lab, Hangzhou, China. His research interests include photoacoustic microscopy, photoacoustic tomography, nuclear magnetic imaging and photoacoustic spectroscopy.